11-13-2017

Measurement and modeling of out-of-field doses from various advanced post-mastectomy radiotherapy techniques

Jihyung Yoon
Louisiana State University

David Heins
Louisiana State University

Xiaodong Zhao
Louisiana State University

Mary Sanders
Mary Bird Perkins Cancer Center

Rui Zhang
Louisiana State University

Recommended Citation

Yoon, J., Heins, D., Zhao, X., Sanders, M., & Zhang, R. (2017). Measurement and modeling of out-of-field doses from various advanced post-mastectomy radiotherapy techniques. *Physics in Medicine and Biology, 62* (23), 9039-9053. https://doi.org/10.1088/1361-6560/aa94b5

HHS Public Access

Author manuscript

Phys Med Biol. Author manuscript; available in PMC 2018 November 13.

Published in final edited form as:

Phys Med Biol. ; 62(23): 9039–9053. doi:10.1088/1361-6560/aa94b5.

Measurement and modeling of out-of-field doses from various advanced post-mastectomy radiotherapy techniques

Jihyung Yoon[1], **David Heins**[1], **Xiaodong Zhao**[1], **Mary Sanders**[2], and **Rui Zhang**[1,2,*]

[1]Medical Physics Program, Department of Physics and Astronomy, Louisiana State University, Baton Rouge, Louisiana, USA

[2]Department of Radiation Oncology, Mary Bird Perkins Cancer Center, Baton Rouge, Louisiana, USA

Abstract

More and more advanced radiotherapy techniques have been adopted for post-mastectomy radiotherapies (PMRT). Patient dose reconstruction is challenging for these advanced techniques because they increase the low out-of-field dose area while the accuracy of out-of-field dose calculations by current commercial treatment planning systems (TPSs) is poor. We aim to measure and model the out-of-field radiation doses from various advanced PMRT techniques. PMRT treatment plans for an anthropomorphic phantom were generated, including volumetric modulated arc therapy (VMAT) with standard and flattening-filter-free (FFF) photon beams, mixed beam therapy, 4-field intensity modulated radiation therapy (IMRT), and Tomotherapy. We measured doses in the phantom where the TPS calculated doses were lower than 5% of the prescription dose using thermoluminescent dosimeters (TLD). The TLD measurements were corrected by two additional energy correction factors, namely out-of-beam out-of-field (OBOF) correction factor K_{OBOF} and in-beam out-of-field (IBOF) correction factor K_{IBOF}, which were determined by separate measurements using an ion chamber and TLD. A simple analytical model was developed to predict out-of-field dose as a function of distance from the field edge for each PMRT technique. The root mean square discrepancies between measured and calculated out-of-field doses were within 0.66 cGy/Gy for all techniques. The IBOF doses were highly scattered and should be evaluated case by case. One can easily combine the measured out-of-field dose here with the in-field dose calculated by the local TPS to reconstruct organ doses for a specific PMRT patient if the same treatment apparatus and technique were used.

Keywords

Post-mastectomy radiotherapy; out-of-field dose; intensity modulated radiotherapy; volumetric modulated arc therapy; flattening-filter-free; mixed beam therapy; Tomotherapy

*Corresponding author: Department of Physics and Astronomy, Louisiana State University, Baton Rouge, LA, USA. rzhang@lsu.edu (R. Zhang). Phone: 225-215-1132.

Conflict of interest statement

The authors have no conflicts of interest.

PACS number: 87.53.Bn, 87.53.Jw, 87.55.D-

1. Introduction

Post-mastectomy radiotherapy (PMRT) is commonly used for patients with invasive breast cancer after surgery to sterilize the residual tumor cells and has been shown to reduce local recurrences and improve the overall survival (EBCTCG *et al.*, 2014). More and more new and advanced radiotherapy technologies have been adopted for PMRT: 4-field intensity modulated radiation therapy (IMRT) was reported to have the best balance of target coverage and normal tissue sparing compared with other PMRT techniques (Wang *et al.*, 2015); bolus electron conformal therapy (BECT) is an effective modality for PMRT, although it can cause dose heterogeneity in some cases (Perkins *et al.*, 2001; Kudchadker *et al.*, 2002); the methodology of BECT combined with IMRT for PMRT has been experimentally confirmed with improved dose homogeneity (Kavanaugh *et al.*, 2013); flattening-filter-free (FFF) beams can potentially reduce the dose to organs at risk (Subramaniam *et al.*, 2012); the current standards of care for PMRT at our institution are volumetric modulated arc therapy (VMAT) and Tomotherapy (Ashenafi *et al.*, 2010; Nichols *et al.*, 2014). Both modalities provide good target coverage and dose homogeneity, but the large cloud of low dose delivered to the normal tissues is of concern (Ashenafi *et al.*, 2010; Nichols *et al.*, 2014).

Radiotherapy can cause a spectrum of acute and chronic side effects for the breast cancer patients (Neugut *et al.*, 1993; Hojris *et al.*, 1999; Gao *et al.*, 2003; Darby *et al.*, 2013; Grantzau *et al.*, 2013). According to the literature (Dorr and Herrmann, 2002; Diallo *et al.*, 2009), the majority of the second cancers were observed in the low or intermediate dose areas. The advanced radiotherapy techniques like IMRT and Tomotherapy will increase the low dose region because of the beam modulation (more monitor units) and the non-opposed beam multiplicity (radiation is more spread out than in conformal radiotherapy). To quantify a patient's risk of developing radiogenic side effects after PMRT, accurate knowledge of the patient dose (both primary and stray radiation doses) is essential. It is generally accepted that commercial treatment planning systems (TPSs) severely underestimate dose at low dose regions (Jang *et al.*, 2008; Howell *et al.*, 2010a; Huang *et al.*, 2013; Joosten *et al.*, 2013; Wang and Ding, 2014; Jagetic and Newhauser, 2015).

Out-of-field dose data based on measurements or Monte Carlo simulations for static and IMRT photon fields were extensively reported in the literature (Stovall *et al.*, 1995; Mutic and Low, 1998; Mutic and Klein, 1999; Stern, 1999; Meeks *et al.*, 2002; Kry *et al.*, 2005; Kry *et al.*, 2006; Sharma *et al.*, 2006; Wang and Xu, 2008; Bednarz and Xu, 2009; Ruben *et al.*, 2011; Halg *et al.*, 2012; Kaderka *et al.*, 2012; La Tessa *et al.*, 2012; Taddei *et al.*, 2013; Covington *et al.*, 2016), while analytical models of out-of-field dose from photon external therapy had only been proposed in a few studies (McParland and Fair, 1992; Taddei *et al.*, 2013; Jagetic and Newhauser, 2015; Hauri *et al.*, 2016). Most of the previous modeling studies focused on open beams or conventional field-in-field beams, and the modeling of IMRT beams required intensive information of each field (Hauri *et al.*, 2016). None of the previous studies proposed any analytical model to calculate out-of-field dose from PMRT techniques.

Therefore, the objective of this study was to measure and model the out-of-field doses from various advanced PMRT techniques. We measured the out-of-field doses by delivering

various PMRT plans to an anthropomorphic phantom loaded with thermoluminescent dosimeter (TLD). We corrected TLD measurements by additional energy correction factors, and developed a simple analytical model to predict out-of-field doses based on the measured data. Calculations of the risk of developing side effects after receiving each PMRT technique or plan quality comparison is beyond the scope of this paper and will be reported in a separate study.

2. Methods and Materials

2.1. Treatment planning

An Atom dosimetry adult male phantom with a breast attachment (CIRS, Inc., Norfork, VA) was used for treatment planning and measurements (figure 1). The phantom is transected in 2.5 cm slices and each slice contains a 1.5 cm^2 grid of holes to hold TLD rods. It was scanned by a GE LightSpeed 16 Slice computed tomography (CT) scanner (GE Healthcare, Little Chalfont, United Kingdom), and the CT images with 2.5 mm slice thickness were imported into Pinnacle 9.8 TPS (Philips Healthcare, Amsterdam, Netherlands). Both planning target volume (PTV) and organs at risk (OARs) were contoured on the phantom and were approved by a board certified radiation oncologist (M Sanders) who is specialized in breast cancer radiation oncology. The PTV included the left chest wall, left supraclavicular area and axillary area, and internal mammary chain area. OARs included bladder, brain, contralateral breast, colon, esophagus, heart, kidney, liver, lung, pharynx, rectum, small intestine, spinal cord, stomach, thyroid and trachea.

Various PMRT treatment plans were generated, including a standard VMAT, two FFF VMAT with 6 MV (6x FFF VMAT) and 10 MV photons (10x FFF VMAT), BECT mixed with IMRT and VMAT beams (mixed beam therapy), 4-field IMRT, and Tomotherapy. The dose prescription was 50Gy administered in 25 fractions for all the plans. The following criteria were met for each treatment plan to be considered clinically acceptable and therefore representative of an actual plan administered to a patient: The volume of the PTV receiving at least 95% of the prescribed dose is greater than or equal to 95% (NRGOncology, 2013); the volume of lungs receiving at least 20 Gy is less than 20% (Marks *et al.*, 2010); the volume of heart receiving at least 22.5 Gy is less than 20% (Hardenbergh *et al.*, 2001).

All the VMAT plans were generated in Pinnacle 9.8 TPS and a dual-arc with 230° rotations (between 180° and 310°) was used to cover the PTV. The beam geometry consisted of a 0 degree couch angle and a 45 degree collimator angle. The same beam setup was used for all VMAT plans, while plan optimization was performed independently using the SmartArc optimization algorithm in Pinnacle. The final plans required 12525 MUs (standard VMAT), 20900 MUs (6x FFF VMAT) and 25525 MUs (10x FFF VMAT).

Mixed beam therapy plan was generated in Pinnacle 9.8 TPS and .decimal p.d TPS (v5.1.9) (.decimal LLC, Sanford, FL), and a single 16 MeV BECT electron beam was used to treat the chest wall (20 fractions), two 10 MV anterior-posterior (AP) and posterior-anterior (PA) IMRT beams were used to treat the supraclavicular area (20 fractions), and a 230° dual-arc 6 MV VMAT (5 fractions) was optimized on top of the dose distribution from the first 20 fractions to treat the whole PTV and improve the dose homogeneity. The p.d TPS was used

to create the electron bolus that provided the best coverage of the distal surface of the BECT PTV by the 90% isodose surface. More details about the mixed beam planning will be reported in a separate study from our group. The final mixed beam plan required 18925 MUs.

4-field IMRT plan was generated in Pinnacle 9.8 and three 6 MV IMRT beams with gantry angles of 295°, 315° and 150° and one 10 MV IMRT beam with gantry angle of 170° were used to cover the whole PTV. The final 4-field IMRT plan required 17200 MUs.

For Tomotherapy, the CT images and contours in Pinnacle were imported into TomoTherapy® Hi·Art TPS (Accuray, Madison, WI) for plan optimization. Parameters for Tomotherapy plan optimization included a pitch of 0.287, a modulation factor of 2.8, 5.02 cm field width, and the final plan required 87525 MUs.

The collapsed cone convolution (CCC) photon dose calculation algorithm (Ahnesjo and Aspradakis, 1999) in Pinnacle with a dose grid of 4×4×4 mm^3 and in TomoTherapy® Hi·Art TPSs with a fine dose grid was used to calculate photon beam doses, and the pencil beam redefinition algorithm (Shiu and Hogstrom, 1991) in the .decimal p.d planning software and the pencil beam algorithm (Hogstrom *et al.*, 1981) in the Pinnacle TPS with a dose grid of 4×4×4 mm^3 were used to calculate electron beam doses. A 1 cm Superflab bolus was placed on the ipsilateral chest wall for all treatment techniques for the purpose of dose buildup except the BECT component of the mixed beam therapy. All the plans were comparable to the standard PMRT patient plans in our clinic and were reviewed and approved by the radiation oncologist.

2.2. Out-of-field dose measurements

2.2.1. TLD dosimetry—TLD dosimeter was used in this study and each TLD rod contained approximately 45 mg TLD-100 (LiF:Mg,Ti) powder. The TLD rods were read using a REXON UL-320 Reader (Rexon Components, Inc., Beachwood, OH). The TLD powder in each rod was divided into three samples of approximately 15 mg each and the three samples were used to determine the mean dose for each TLD rod. All TLDs were stored for two days before reading to minimize the fading effect.

The literature showed that commercial TPSs cannot calculate dose accurately at low out-of-field dose regions (<5% of prescription dose) (Howell *et al.*, 2010a; Wang and Ding, 2014), and the TLD measurement points in this study were therefore chosen at places where TPS calculated doses were lower than 5% isodose. The measurement points in OARs were selected uniformly in each organ, and the same measurement points were used for all the PMRT techniques throughout this study. TLD was not placed at a certain point if the TPS calculated dose at that point was in-field (greater than 5 % isodose) for a given PMRT technique. Since contralateral breast attachment has no TLD holes, 5 TLD packets (approximately 1×1×0.2 cm^3) were placed on the surface of the breast attachment and another 5 packets were placed between the breast attachment and the phantom. Table 1 shows the number of TLDs used in different organs for each plan, and it does not list stomach because stomach was almost completely in field for all the PMRT techniques.

After measurement points were determined and TLD rods were loaded in the phantom, the phantom was irradiated for each PMRT technique. All VMAT plans, mixed beam therapy (IMRT with additional VMAT) and 4-field IMRT were delivered by Elekta Versa HD™ with a 160-leaf Agility multi-leaf collimator (MLC) (Elekta, Crawley, United Kingdom) which was calibrated according to the American Association of Physicists in Medicine (AAPM) Task Group 51 calibration protocol (Almond *et al.*, 1999). Electron component of the mixed beam therapy was not delivered because out-of-field dose contribution from electron beam is considered to be negligible. Tomotherapy was delivered by TomoTherapy® (Accuray, Madison, WI) which was calibrated according to the AAPM Task Group 148 calibration protocol (Langen *et al.*, 2010). For plans with multiple beam energies such as 4-field IMRT and mixed beam therapy, we performed separate TLD calibrations and measurements for each photon energy since TLD response is energy dependent: we delivered beams with one energy to the anthropomorphic phantom loaded with TLD rods first, did TLD calibration for that energy, unloaded the phantom and plugged in new TLD rods and delivered beams with another energy, did TLD calibration for the new energy. As for TLD calibrations, we sandwiched a TLD packet in solid water phantoms, delivered a known dose to the TLD packet using the radiation beam of a specified energy, and recorded the TLD reading. This was repeated for several dose levels and a calibration curve was created based on the readings. The total TLD dose was calculated by summing doses from all energies. To ensure sufficient linearity in TLD response, we delivered four fractions with 2 Gy per fraction, which would deliver approximately 40 cGy at 5 % isodose line. The uncertainty of the dose measured by each TLD is ≤ 4% according to the literature (Kirby *et al.*, 1992; Ito *et al.*, 2011).

2.2.2. TLD out-of-field energy corrections—It is known that TLD response in the out-of-field region needs additional energy corrections due to the change of incident spectrum of photons (Scarboro *et al.*, 2011; Mijnheer *et al.*, 2013). The TLD dose was calculated as following:

$$D = T \times S \times K_L \times K_{OBOF} \quad (1)$$

where D is the absorbed dose, T is the raw TLD reading, S is the system sensitivity factor, K_L is the linearity correction factor, K_{OBOF} is out-of-beam out-of-field energy correction factor, which means this correction factor applies to the area that is not only out of the high dose region but also out of the path of any radiation beam. The reason we define this TLD correction factor as K_{OBOF} instead of the previously used K_{NR} (non-reference energy correction factor) (Scarboro *et al.*, 2011) is that we want to distinguish it from the in-beam out-of-field correction factor (K_{IBOF}) defined later in this section. Scarboro et al. (2011) measured K_{NR} factors, which are the same as K_{OBOF} in this study, for 6 MV open photon beams and their correction factor ranged from 0.88 to 0.99. For IMRT beams and higher photon energies, however, this information is lacking.

For rotational radiotherapies like VMAT or Tomotherapy, a point can be in the low dose region but is located within the path of the theoretically rotational open beam coming from the widest jaw opening in the plan. There is a little dose contribution from the primary beam

incident toward the point because there is a minimum gap limit between the opposing MLCs, although the point is blocked by the MLCs most of the time due to beam modulation. This point can be regarded as in-beam out-of-field (IBOF), as shown in figure 2. For this region, TLD correction factor should be different from OBOF region because energy spectrum here contains more high energy components and Eq. (1) should be replaced by

$$D = T \times S \times K_L \times K_{IBOF} \quad (2)$$

For open field and fixed-beam IMRT, K_{IBOF} should not be used because out-of-field region (< 5% of prescription dose) is always outside the path of beams coming from the maximum collimator openings.

In this study, ion chamber (IC) measurement was used as the reference dosimeter since the nominal photon energy range for the PTW Farmer-type IC (N30013 PTW Farmer® Ionization Chamber, PTW, Freiburg, Germany) has the lower end as 30 keV, while it was reported that mean photon energy at out-of-field location was greater than 170 keV for 6 MV photon beams (Scarboro *et al.*, 2011), which is significantly higher than the lower limit of the IC. Therefore IC's over-response in the out-of-field region is negligible, which is also consistent with the literature (Kry *et al.*, 2017). To quantify K_{OBOF} and K_{IBOF} for all PMRT techniques, we transferred PMRT treatment plans from the anthropomorphic phantom to a water phantom in Pinnacle TPS and performed out-of-field dose measurements with TLDs and an IC in solid water phantoms. For VMAT and mixed beam therapy plans, OBOF doses were measured at 23, 28 and 33 cm away from the beam axis and at 5 and 10 cm depths (in AP direction) (figure 2). IBOF doses were measured at 6 and 10 cm from beam axis and at 10 and 15 cm depths (in AP direction) in the phantom and we made sure the doses at those IBOF points were lower than 5% of prescription dose by checking the dose distribution in TPS (figure 2). For IMRT plans (4-field IMRT), OBOF doses were measured at 21.5, 25 and 30 cm away from the beam axis and at 5 and 10 cm depths (in AP direction) and there was no IBOF point for 4-field IMRT beams. The measurement results were used to obtain K_{OBOF} and K_{IBOF} for a given PMRT technique, and they can be calculated as the ratio of measured doses from IC and TLD.

TLD measurement points were separated into two groups: OBOF and IBOF. For each group, K_{OBOF} and K_{IBOF} correction factors were applied accordingly.

2.3. Out-of-field dose modeling

A simple analytical model was used to fit the out-of-field dose data and the model was chosen based on the best balance between accuracy and complexity. The expected dose at the out-of-field points (D_{OF}) can be calculated by

$$D_{OF} = D_{RX} \times \left[\frac{C_1}{(d+t)^2} - \frac{C_2}{(d+t)} + C_3 \right], \quad (3)$$

where D_{RX} is the prescription dose, d is the distance from the field edge (50% isodose line) in mm unit, C_1, C_2, C_3 and t are the fitting parameters determined by each treatment technique.

In Pinnacle, we first created a contour based on 50% isodose surface for the anthropomorphic phantom, and identified TLD hole positions on each slice. We then exported the 50% contour as a DICOM format and imported it into MATLAB. The distance from the 50% contour to each TLD measurement point was calculated by seeking the minimum distance from all points in the 50% surface to the TLD location. The fitting parameters were adjusted by minimizing the total root mean square deviation (RMSD)

$$RMSD=\sqrt{\frac{\sum_{i=1}^{n}(D_{i,model}-D_{i,measurement})^2}{n}}. \quad (4)$$

for each TLD location, i, evaluated for n TLD locations.

2.4. Mean organ dose reconstruction and comparison with TPS calculations

To further illustrate the necessity of the investigation of the out-of-field doses from various PMRT techniques, the mean organ doses were reconstructed based on a volume-weighting method (Howell *et al.*, 2010b) and were compared with the organ doses predicted by the TPS alone: each organ volume (V_{organ}) was divided by 5% isodose line based on the TPS calculated dose, such as greater than 5% ($V_{organ}^{>5\%}$) and lower than 5% ($V_{organ}^{<5\%}$) of prescription dose. For the region $V_{organ}^{<5\%}$, corrected TLD doses from equation (1, 2) in the corresponding organ were averaged ($D_{TLD}^{<5\%}$). Otherwise, TPS predicted average dose $D_{TPS}^{>5\%}$ in the volume was used for the region $V_{organ}^{>5\%}$. The mean organ dose (D_{organ}) was reconstructed by a volume-weighting equation

$$D_{organ}=\frac{V_{organ}^{>5\%}}{V_{organ}}\times D_{TPS}^{>5\%}+\frac{V_{organ}^{<5\%}}{V_{organ}}\times D_{TLD}^{<5\%} \quad (5)$$

Although 8 Gy was delivered to the phantom to ensure TLD linearity, the final organ doses were scaled to the prescription dose of 50 Gy since this is the standard prescription for PMRT patients. The mean organ doses calculated by the TPS alone were also extracted for comparison.

3. Results

It was found that the additional TLD correction factors (K_{OBOF} and K_{IBOF}) have little dependence on off-axis distance or depth for the same technique. For simplicity, the average values were used as the correction factors for each PMRT technique (table 2). The K_{IBOF} factor was always 1.0, which revealed the photon energy is high in the IBOF region and the

additional TLD energy correction is not necessary in these areas for the PMRT techniques evaluated in this study. The same K_{OBOF} for 6x FFF VMAT was used for Tomotherapy considering the similarity between these two rotational techniques.

Figure 3 shows measured out-of-field doses versus distance from the field edge for different PMRT techniques and the doses were scaled up to match the prescription dose of 50 Gy. For VMAT plans (figure 3(a–c)), doses at IBOF points (open circles) showed a different pattern from OBOF points (solid circles) since they were exposed to the primary beams during gantry rotation. For mixed beam therapy, there were no pure IBOF points because IBOF points for VMAT beam were OBOF points for supraclavicular IMRT beams. The doses at IBOF+OBOF points (figure 3(d), open triangle) were much closer to doses at OBOF points. For 4-field IMRT (figure 3(e)), all the measurement points were OBOF points. For Tomotherapy (figure 3(f)), there were no IBOF measurements since all potential IBOF locations were within the 5% prescription isodose line. Also, the measured doses were scattered and higher than the others near the field edge. Except for Tomotherapy, the number of MU used in each PMRT technique was not correlated with the out-of-field doses or organ doses.

The analytical model was used to fit the measured out-of-field data and the dose curves predicted by the model were plotted in figure 3 along with the measured data. The model parameter values and the RMSD (in cGy/Gy) between measured and calculated doses for each treatment technique were listed in table 3. Only OBOF doses were used in the fittings except “mixed beam therapy-2nd fit” in which IBOF+OBOF points were also included because they were close to OBOF doses. The dashed line in figure 3(d) represented this second fit and the RMSD increased compared to the first fit as shown in table 3. As shown in figure 3(a–c), the doses at IBOF points from VMAT plans were highly scattered and did not follow any obvious trend, and a model fit for these locations was therefore not attempted.

Based on equation (5), mean organ doses were reconstructed and shown in table 4. Stomach was not shown here because TLD measurements were not performed. Mean organ doses calculated by Pinnacle TPS were also listed in the table and the agreement between TPS calculations and those based on the new method was poor. TPS underestimated organ doses in most cases and the discrepancy was up to 2.3 cGy/Gy.

4. Discussion

In this study, we measured out-of-field doses from various advanced PMRT techniques, and also developed a simple analytical model to predict out-of-field doses for each technique. Our results show that OBOF doses from different PMRT techniques approximately follow a simple polynomial model, while IBOF doses from rotational therapy like VMAT were highly scattered because the IBOF region was exposed to the rotational narrow open beam and the dose is mainly determined by the exposure time and dose rate. The TPS underestimated the out-of-field doses and organ doses in most cases.

As we mentioned previously, the out-of-field data from advanced PMRT were largely lacking in the literature and comparing our data or model with previous studies is difficult

because the out-of-field dose depends on treatment machine and techniques. Despite that, some of our qualitative findings agreed with previous studies: TPS systematically underestimates out-of-field doses; the K_{OBOF} values for 6MV photon beams are consistent with the previous study (Scarboro *et al.*, 2011); Tomotherapy has higher out-of-field doses at most locations compared to other techniques (Mutic and Low, 1998; Meeks *et al.*, 2002; Xu *et al.*, 2008). This can be explained by the fact that radiation was not limited enough due to the characteristic of Tomotherapy (the beam is continuously delivered from 360 degrees around the phantom and more MU is used) and possibly less peripheral shielding in Tomotherapy units; dosimetric results between standard and FFF beams were comparable for breast radiotherapies (Subramaniam *et al.*, 2012; Spruijt *et al.*, 2013; Wang *et al.*, 2014), although Subramaniam et al. (2012) claimed some improved sparing of contralateral organs with FFF beams which was not observed in this study. This was possibly because the out-of-field doses were not considered in their work, and different treatment machines and plan optimization methods were used in the two studies.

Our study has several particular strengths. First, to the best knowledge of the authors', we measured and compared the out-of-field doses for various advanced PMRT technique for the first time. Second, we corrected the TLD measurements with additional energy correction factors. We introduced a new TLD correction factor, K_{IBOF}, which will improve the accuracy of out-of-field dose measurement and calculation for rotational radiotherapies like VMAT and Tomotherapy. Third, a simple analytical model was developed to predict the out-of-field doses from those advanced PMRT techniques with a reasonable accuracy. This model can be used in the clinic directly while the more sophisticated model (Hauri *et al.*, 2016) may need more time to be implemented for clinical usage.

One limitation of our study is that out-of-field doses in figure 3 and organ doses in table 4 were based on measurements within a generic phantom, while the actual dose delivered to a real patient may be different from this study. As we mentioned in the introduction section, our goal is to measure and model the out-of-field doses, and table 4 was only used to demonstrate the necessity of using an improved way to determine out-of-field doses and calculate organ doses. Most real PMRT patients only have CT images from mouth to upper abdomen and it is impossible to reconstruct all the organ doses like what was done for this phantom. Also considering the relatively low magnitude of out-of-field dose and the small variation of photon energy spectra with field size and depth (Xu *et al.*, 2008; Scarboro *et al.*, 2011), the absolute difference between the measured out-of-field doses here and the actual out-of-field dose delivered to the patients is small. One can easily combine the measured out-of-field dose here by looking up the out-of-field dose versus distance curves with the in-field dose calculated by the local TPS to reconstruct organ doses for any PMRT patient if they use the same treatment apparatuses and techniques used in this study. Second, we did not measure the out-of-field dose from the electron component of the mixed beam therapy, while the bremsstrahlung photon tail for 16 MeV electron beam is on the order of 3~4% of the maximum dose. This x-ray contamination could slightly increase ipsilateral lung dose and stomach dose since they are in the direction of the electron beam. The effect on other organ doses should be negligible. Finally, we only measured the additional TLD correction factors (K_{OBOF} and K_{IBOF}) for the PMRT techniques used in this study, while these corrections factor may vary for other treatment techniques and beam energies.

Comprehensive evaluation of these correction factors in various conditions will be the next logical step of our research.

5. Conclusion

In summary, we have measured out-of-field doses for various advanced PMRT techniques using TLDs, proposed and measured additional TLD correction factors using TLDs and an IC, and found the TPS underestimated the out-of-field doses and organ doses in most cases. A simple analytical model was developed and could be used to predict the out-of-field doses for each PMRT technique. Based on our findings, it is necessary to determine out-of-field doses and use a hybrid approach to correctly reconstruct normal tissue doses for PMRT patients. We focused on PMRT only and did not investigate other types of breast cancer radiotherapies because of time and resource limitations. Investigation of out-of-field doses from breast conserving radiotherapies will broaden the generality of the methodology developed in this study, and this work is currently underway in our laboratory.

References

Ahnesjo A, Aspradakis MM. Dose calculations for external photon beams in radiotherapy. Phys Med Biol. 1999; 44:R99–155. [PubMed: 10588277]

Almond PR, Biggs PJ, Coursey BM, Hanson WF, Huq MS, Nath R, Rogers DW. AAPM's TG-51 protocol for clinical reference dosimetry of high-energy photon and electron beams. Med Phys. 1999; 26:1847–70. [PubMed: 10505874]

Ashenafi M, Boyd RA, Lee TK, Lo KK, Gibbons JP, Rosen, Fontenot JD, Hogstrom KR. Feasibility of postmastectomy treatment with helical TomoTherapy. Int J Radiat Oncol Biol Phys. 2010; 77:836–42. [PubMed: 19879697]

Bednarz B, Xu XG. Monte Carlo modeling of a 6 and 18 MV Varian Clinac medical accelerator for in-field and out-of-field dose calculations: development and validation. Phys Med Biol. 2009; 54:N43–57. [PubMed: 19141879]

Covington EL, Ritter TA, Moran JM, Owrangi AM, Prisciandaro JI. Technical Report: Evaluation of peripheral dose for flattening filter free photon beams. Med Phys. 2016; 43:4789. [PubMed: 27487896]

Darby SC, Ewertz M, McGale P, Bennet AM, Blom-Goldman U, Bronnum D, Correa C, Cutter D, Gagliardi G, Gigante B, Jensen MB, Nisbet A, Peto R, Rahimi K, Taylor C, Hall P. Risk of ischemic heart disease in women after radiotherapy for breast cancer. N Engl J Med. 2013; 368:987–98. [PubMed: 23484825]

Diallo I, Haddy N, Adjadj E, Samand A, Quiniou E, Chavaudra J, Alziar I, Perret N, Guerin S, Lefkopoulos D, de Vathaire F. Frequency distribution of second solid cancer locations in relation to the irradiated volume among 115 patients treated for childhood cancer. Int J Radiat Oncol Biol Phys. 2009; 74:876–83. [PubMed: 19386434]

Dorr W, Herrmann T. Cancer induction by radiotherapy: dose dependence and spatial relationship to irradiated volume. J Radiol Prot. 2002; 22:A117–21. [PubMed: 12400959]

EBCTCG, McGale P, Taylor C, Correa C, Cutter D, Duane F, Ewertz M, Gray R, Mannu G, Peto R, Whelan T, Wang Y, Wang Z, Darby S. Effect of radiotherapy after mastectomy and axillary surgery on 10-year recurrence and 20-year breast cancer mortality: meta-analysis of individual patient data for 8135 women in 22 randomised trials. Lancet. 2014; 383:2127–35. [PubMed: 24656685]

Gao X, Fisher SG, Emami B. Risk of second primary cancer in the contralateral breast in women treated for early-stage breast cancer: a population-based study. Int J Radiat Oncol Biol Phys. 2003; 56:1038–45. [PubMed: 12829139]

Grantzau T, Mellemkjaer L, Overgaard J. Second primary cancers after adjuvant radiotherapy in early breast cancer patients: a national population based study under the Danish Breast Cancer Cooperative Group (DBCG). Radiother Oncol. 2013; 106:42–9. [PubMed: 23395067]

Halg RA, Besserer J, Schneider U. Systematic measurements of whole-body dose distributions for various treatment machines and delivery techniques in radiation therapy. Med Phys. 2012; 39:7662–76. [PubMed: 23231314]

Hardenbergh PH, Munley MT, Bentel GC, Kedem R, Borges-Neto S, Hollis D, Prosnitz LR, Marks LB. Cardiac perfusion changes in patients treated for breast cancer with radiation therapy and doxorubicin: preliminary results. Int J Radiat Oncol Biol Phys. 2001; 49:1023–8. [PubMed: 11240243]

Hauri P, Halg RA, Besserer J, Schneider U. A general model for stray dose calculation of static and intensity-modulated photon radiation. Med Phys. 2016; 43:1955. [PubMed: 27036591]

Hogstrom KR, Mills MD, Almond PR. Electron beam dose calculations. Phys Med Biol. 1981; 26:445–59. [PubMed: 6787621]

Hojris I, Overgaard M, Christensen JJ, Overgaard J. Morbidity and mortality of ischaemic heart disease in high-risk breast-cancer patients after adjuvant postmastectomy systemic treatment with or without radiotherapy: analysis of DBCG 82b and 82c randomised trials. Radiotherapy Committee of the Danish Breast Cancer Cooperative Group. Lancet. 1999; 354:1425–30. [PubMed: 10543669]

Howell RM, Scarboro SB, Kry SF, Yaldo DZ. Accuracy of out-of-field dose calculations by a commercial treatment planning system. Phys Med Biol. 2010a; 55:6999–7008. [PubMed: 21076191]

Howell RM, Scarboro SB, Taddei PJ, Krishnan S, Kry SF, Newhauser WD. Methodology for determining doses to in-field, out-of-field and partially in-field organs for late effects studies in photon radiotherapy. Phys Med Biol. 2010b; 55:7009–23. [PubMed: 21076193]

Huang JY, Followill DS, Wang XA, Kry SF. Accuracy and sources of error of out-of field dose calculations by a commercial treatment planning system for intensity-modulated radiation therapy treatments. J Appl Clin Med Phys. 2013; 14:4139. [PubMed: 23470942]

Ito S, Parker BC, Levine R, Sanders ME, Fontenot J, Gibbons J, Hogstrom K. Verification of calculated skin doses in postmastectomy helical tomotherapy. Int J Radiat Oncol Biol Phys. 2011; 81:584–91. [PubMed: 21300469]

Jagetic LJ, Newhauser WD. A simple and fast physics-based analytical method to calculate therapeutic and stray doses from external beam, megavoltage x-ray therapy. Phys Med Biol. 2015; 60:4753–75. [PubMed: 26040833]

Jang SY, Liu HH, Mohan R. Underestimation of low-dose radiation in treatment planning of intensity-modulated radiotherapy. Int J Radiat Oncol Biol Phys. 2008; 71:1537–46. [PubMed: 18513883]

Joosten A, Matzinger O, Jeanneret-Sozzi W, Bochud F, Moeckli R. Evaluation of organ-specific peripheral doses after 2-dimensional, 3-dimensional and hybrid intensity modulated radiation therapy for breast cancer based on Monte Carlo and convolution/superposition algorithms: implications for secondary cancer risk assessment. Radiother Oncol. 2013; 106:33–41. [PubMed: 23351844]

Kaderka R, Schardt D, Durante M, Berger T, Ramm U, Licher J, La Tessa C. Out-of-field dose measurements in a water phantom using different radiotherapy modalities. Phys Med Biol. 2012; 57:5059–74. [PubMed: 22836598]

Kavanaugh JA, Hogstrom KR, Chu C, Carver RA, Fontenot JP, Henkelmann G. Delivery confirmation of bolus electron conformal therapy combined with intensity modulated x-ray therapy. Med Phys. 2013; 40:021724. [PubMed: 23387747]

Kirby TH, Hanson WF, Johnston DA. Uncertainty analysis of absorbed dose calculations from thermoluminescence dosimeters. Med Phys. 1992; 19:1427–33. [PubMed: 1461205]

Kry SF, Bednarz B, Howell RM, Dauer L, Followill D, Klein E, Paganetti H, Wang B, Wuu CS, George Xu X. AAPM TG 158: Measurement and calculation of doses outside the treated volume from external-beam radiation therapy. Med Phys. 2017 [Epub ahead of print].

Kry SF, Salehpour M, Followill DS, Stovall M, Kuban DA, White RA, Rosen. Out-of-field photon and neutron dose equivalents from step-and-shoot intensity-modulated radiation therapy. Int J Radiat Oncol Biol Phys. 2005; 62:1204–16. [PubMed: 15990026]

Kry SF, Titt U, Ponisch F, Followill D, Vassiliev ON, White RA, Mohan R, Salehpour M. A Monte Carlo model for calculating out-of-field dose from a varian 6 MV beam. Med Phys. 2006; 33:4405–13. [PubMed: 17153419]

Kudchadker RJ, Hogstrom KR, Garden AS, McNeese MD, Boyd RA, Antolak JA. Electron conformal radiotherapy using bolus and intensity modulation. Int J Radiat Oncol Biol Phys. 2002; 53:1023–37. [PubMed: 12095572]

La Tessa C, Berger T, Kaderka R, Schardt D, Korner C, Ramm U, Licher J, Matsufuji N, Vallhagen Dahlgren C, Lomax T, Reitz G, Durante M. Out-of-field dose studies with an anthropomorphic phantom: comparison of X-rays and particle therapy treatments. Radiother Oncol. 2012; 105:133–8. [PubMed: 22575675]

Langen KM, Papanikolaou N, Balog J, Crilly R, Followill D, Goddu SM, Grant W 3rd, Olivera G, Ramsey CR, Shi C. QA for helical tomotherapy: report of the AAPM Task Group 148. Med Phys. 2010; 37:4817–53. [PubMed: 20964201]

Marks LB, Bentzen SM, Deasy JO, Kong FM, Bradley JD, Vogelius IS, El Naqa I, Hubbs JL, Lebesque JV, Timmerman RD, Martel MK, Jackson A. Radiation dose-volume effects in the lung. Int J Radiat Oncol Biol Phys. 2010; 76:S70–6. [PubMed: 20171521]

McParland BJ, Fair HI. A method of calculating peripheral dose distributions of photon beams below 10 MV. Med Phys. 1992; 19:283–93. [PubMed: 1584119]

Meeks SL, Paulino AC, Pennington EC, Simon JH, Skwarchuk MW, Buatti JM. In vivo determination of extra-target doses received from serial tomotherapy. Radiother Oncol. 2002; 63:217–22. [PubMed: 12063012]

Mijnheer B, Beddar S, Izewska J, Reft C. In vivo dosimetry in external beam radiotherapy. Med Phys. 2013; 40:070903. [PubMed: 23822404]

Mutic S, Klein EE. A reduction in the AAPM TG-36 reported peripheral dose distributions with tertiary multileaf collimation. American Association of Physicists in Medicine Task Group 36. Int J Radiat Oncol Biol Phys. 1999; 44:947–53. [PubMed: 10386654]

Mutic S, Low DA. Whole-body dose from tomotherapy delivery. Int J Radiat Oncol Biol Phys. 1998; 42:229–32. [PubMed: 9747842]

Neugut AI, Robinson E, Lee WC, Murray T, Karwoski K, Kutcher GJ. Lung cancer after radiation therapy for breast cancer. Cancer. 1993; 71:3054–7. [PubMed: 8490833]

Nichols GP, Fontenot JD, Gibbons JP, Sanders ME. Evaluation of volumetric modulated arc therapy for postmastectomy treatment. Radiat Oncol. 2014; 9:66. [PubMed: 24571913]

NRGOncology. Standard or Comprehensive Radiation Therapy in Treating Patients with Early-Stage Breast Cancer Previously Treated with Chemotherapy and Surgery. 2013

Perkins GH, McNeese MD, Antolak JA, Buchholz TA, Strom EA, Hogstrom KR. A custom three-dimensional electron bolus technique for optimization of postmastectomy irradiation. Int J Radiat Oncol Biol Phys. 2001; 51:1142–51. [PubMed: 11704339]

Ruben JD, Lancaster CM, Jones P, Smith RL. A comparison of out-of-field dose and its constituent components for intensity-modulated radiation therapy versus conformal radiation therapy: implications for carcinogenesis. Int J Radiat Oncol Biol Phys. 2011; 81:1458–64. [PubMed: 20950947]

Scarboro SB, Followill DS, Howell RM, Kry SF. Variations in photon energy spectra of a 6 MV beam and their impact on TLD response. Med Phys. 2011; 38:2619–28. [PubMed: 21776799]

Sharma SD, Upreti RR, Deshpande DD. Use of peripheral dose data from uniform dynamic multileaf collimation fields to estimate out-of-field organ dose in patients treated employing sliding window intensity-modulated radiotherapy. Phys Med Biol. 2006; 51:2987–95. [PubMed: 16723779]

Shiu AS, Hogstrom KR. Pencil-beam redefinition algorithm for electron dose distributions. Med Phys. 1991; 18:7–18. [PubMed: 2008174]

Spruijt KH, Dahele M, Cuijpers JP, Jeulink M, Rietveld D, Slotman BJ, Verbakel WF. Flattening filter free vs flattened beams for breast irradiation. Int J Radiat Oncol Biol Phys. 2013; 85:506–13. [PubMed: 22672750]

Stern RL. Peripheral dose from a linear accelerator equipped with multileaf collimation. Med Phys. 1999; 26:559–63. [PubMed: 10227359]

Stovall M, Blackwell CR, Cundiff J, Novack DH, Palta JR, Wagner LK, Webster EW, Shalek RJ. Fetal dose from radiotherapy with photon beams: report of AAPM Radiation Therapy Committee Task Group No. 36. Med Phys. 1995; 22:63–82. [PubMed: 7715571]

Subramaniam S, Thirumalaiswamy S, Srinivas C, Gandhi GA, Kathirvel M, Kumar KK, Mallik S, Babaiah M, Pawar Y, Clivio A, Fogliata A, Mancosu P, Nicolini G, Vanetti E, Cozzi L. Chest wall radiotherapy with volumetric modulated arcs and the potential role of flattening filter free photon beams. Strahlenther Onkol. 2012; 188:484–90. [PubMed: 22402870]

Taddei PJ, Jalbout W, Howell RM, Khater N, Geara F, Homann K, Newhauser WD. Analytical model for out-of-field dose in photon craniospinal irradiation. Phys Med Biol. 2013; 58:7463–79. [PubMed: 24099782]

Wang B, Xu XG. Measurements of non-target organ doses using MOSFET dosemeters for selected IMRT and 3D CRT radiation treatment procedures. Radiat Prot Dosimetry. 2008; 128:336–42. [PubMed: 17627959]

Wang J, Li X, Deng Q, Xia B, Wu S, Liu J, Ma S. Postoperative radiotherapy following mastectomy for patients with left-sided breast cancer: A comparative dosimetric study. Medical dosimetry: official journal of the American Association of Medical Dosimetrists. 2015; 40:190–4. [PubMed: 25534167]

Wang L, Ding GX. The accuracy of the out-of-field dose calculations using a model based algorithm in a commercial treatment planning system. Phys Med Biol. 2014; 59:N113–28. [PubMed: 24925858]

Wang Y, Vassil A, Tendulkar R, Bayouth J, Xia P. Feasibility of using nonflat photon beams for whole-breast irradiation with breath hold. J Appl Clin Med Phys. 2014; 15:4397. [PubMed: 24423835]

Xu XG, Bednarz B, Paganetti H. A review of dosimetry studies on external-beam radiation treatment with respect to second cancer induction. Phys Med Biol. 2008; 53:R193–241. [PubMed: 18540047]

Figure 1.
An Atom dosimetry phantom with a contralateral breast attachment on the right and a bolus used in this study to cover the irradiated area on the left.

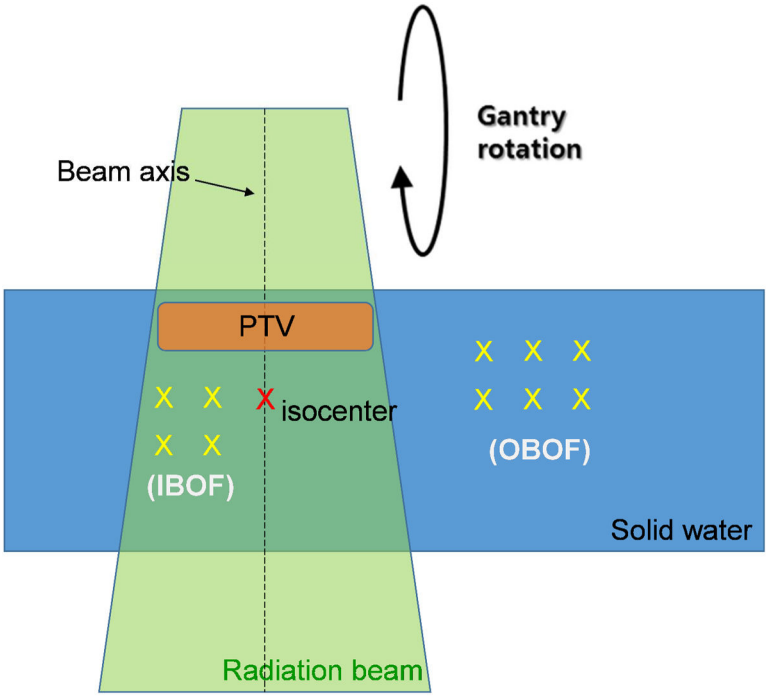

Figure 2.

A schematic diagram of out-of-beam out-of-field (OBOF) and in-beam out-of-field (IBOF) energy correction factors measurement setup. TLD and IC were located at the yellow marks and the red mark represents the isocenter. A VMAT plan delivery is shown here with gantry rotating in a cross-plane direction. The IMRT plan is not shown here and only OBOF measurements were performed for IMRT beams.

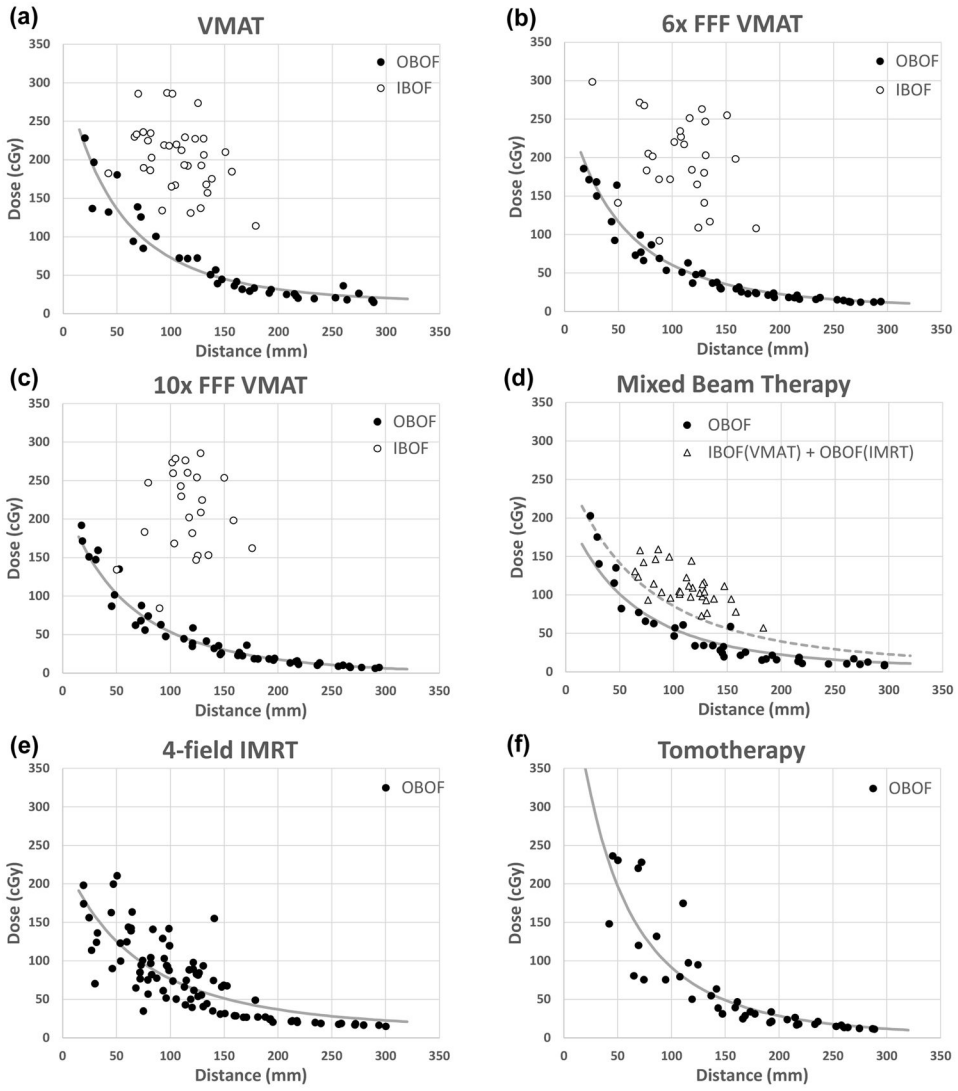

Figure 3.

Measured out-of-field doses versus distance from the field edge for various PMRT treatment techniques overlaid by the analytical model fit to the measured data. Only OBOF doses were used in the fittings except the second fit of mixed beam therapy doses in which IBOF +OBOF points were also included. The dashed line in figure 3(d) represented this second fit.

Table 1

Number of TLDs used in organs at risk for different PMRT techniques. TLD was not placed in some organs for certain techniques because the entire organ was in field (covered by the 5% isodose line). (CL Breast: contralateral breast)

Organ	VMAT	6x FFF VMAT	10x FFF VMAT	Mixed beam therapy	4-field IMRT	Tomotherapy
Bladder	4	4	4	4	4	4
Brain	4	4	4	4	4	4
CL Breast	14	14	14	14	14	10
Colon	8	17	17	17	17	17
Esophagus	3	2	1	3	6	0
Heart	5	2	0	5	7	0
Left kidney	1	1	1	1	1	0
Liver	4	6	2	5	6	0
Lung	14	11	13	15	15	0
Pharynx	2	2	2	2	2	2
Rectum	2	2	2	2	2	2
Right kidney	2	2	2	2	2	0
Small intestine	8	8	8	8	8	8
Spinal Cord	7	5	6	7	7	4
Thyroid	1	2	3	1	3	0
Trachea	1	1	1	1	1	0

Table 2

Mean out-of-beam out-of-field correction factor (K_{OBOF}) and in-beam out-of-field correction factor (K_{IBOF}) for different PMRT techniques. Dashed table entry indicates the correction does not apply to that technique. The standard deviation (σ) is reported as one standard deviation of the mean.

PMRT Technique	TLD correction factors	
	K_{OBOF} (σ)	K_{IBOF} (σ)
VMAT	0.93 (0.02)	1.0 (0.01)
6x FFF VMAT	0.87 (0.02)	1.0 (0.01)
10x FFF VMAT	0.84 (0.01)	1.0 (0.01)
Mixed beam therapy	0.88 (0.01)	1.0 (0.01)
4-field IMRT	0.83 (0.01)	-

Table 3

Fitting parameters for the analytical model and root mean square deviation (RMSD) between the model calculated and the measured data for different PMRT techniques. Only OBOF doses were used in the fittings except “mixed beam therapy-2nd fit” in which IBOF+OBOF points were also included in the fitting.

	Coefficients				
PMRT Technique	C_1	C_2	C_3	t (mm)	**RMSD (cGy/Gy)**
VMAT	1130	3.45	0.0058	113	0.33
6x FFF VMAT	1000	2.72	0.0031	115	0.22
10x FFF VMAT	1100	2.67	0.0015	130	0.20
Mixed Beam Therapy-1st fit	1290	3.5	0.0037	143	0.39
Mixed Beam Therapy-2nd fit	1810	3.4	0.0034	160	0.63
4-field IMRT	1510	2.9	0.0036	156	0.59
Tomotherapy	1170	3.25	0.003	90	0.66

Table 4

Values of mean organ doses for the CIRS phantom for various PMRT techniques, calculated based on the new volume-weighting method (New) and by the TPS alone (TPS). Prescription dose was 50 Gy for all techniques. (CL Breast: contralateral breast)

OAR	Mean organ dose (cGy)											
	VMAT		6xFFF VMAT		10xFFF VMAT		Mixed beam therapy		4-field IMRT		Tomotherapy	
	TPS	New	TPS	New	TPS	New	TPS	New	TPS	New	TPS	New
Bladder	0	20.7	0	13.1	0	7.3	0	10.6	0	17.1	8.8	13.1
Brain	0	31.6	0	23.9	0	20.3	0	24.6	0	26.2	19.3	23.1
CL Breast	154.1	185.0	111	141.8	159.9	177.2	156.7	178.1	164.8	277.8	425.5	431.4
Colon	49.8	56.5	36.5	41.5	31.5	38.1	51.7	44.2	21	41.7	78.6	94.4
Esophagus	443.8	455.2	482.2	484.9	647	641.4	327.1	342.1	222.8	230.0	1051.5	1051.5
Heart	661.4	665.3	798.6	810.3	970.5	970.5	1176.7	1170.7	573.1	573.8	708.5	708.5
Left Kidney	352.5	348.7	283.4	267.9	354	348.4	389.3	368.1	162	133.9	1647.8	1647.8
Liver	488.3	509.5	403.3	427.8	579.5	587.3	339.1	321.9	281.1	270.9	1640.6	1640.6
Lung	1027.9	1043.3	1071.1	1087.7	1136.1	1156.6	1409.7	1409.9	904.9	902.5	1234.1	1234.1
Pharynx	72	113.0	60.4	94.9	50.8	74.4	54.5	96.3	0	77.3	118.2	126.5
Rectum	0	25.5	0	12.5	0	7.8	0	12.5	0	16.6	8.6	12.2
Right Kidney	156.8	181.3	141.4	154.3	195	212.1	165.4	179.4	41.6	108.3	1611.7	1611.7
Small intestine	34.5	57.9	26.2	41.3	22.7	34.7	36.5	47.6	6.7	39.0	62.4	84.5
Spinal Cord	201.7	222.5	181.4	160.2	254.7	266.6	228.2	214.5	60.3	67.1	290.6	296.1
Thyroid	663.7	639.0	581.2	570.8	542.7	541.5	482	455.8	287.4	279.8	1239.4	1239.4
Trachea	421.9	449.1	493.5	505.1	555.2	567.6	376.4	406.4	191.1	234.2	1021.8	1021.8